

Copyright 2016, ABRACO

Trabalho apresentado durante o INTERCORR 2016, em Búzios/RJ no mês de maio de 2016.

As informações e opiniões contidas neste trabalho são de exclusiva responsabilidade do(s) autor(es).

## **The influence of microstructure and heat treatment of API X52 carbon steel on hydrogen diffusion**

Rhuã C. Souza<sup>a</sup>, Luciano R. Pereira<sup>b</sup>, Lucas M. Starling<sup>c</sup>, José A. C. Ponciano<sup>d</sup>, Alysson H. S. Bueno<sup>e</sup>

### **Abstract**

The objective of this research was to evaluate the susceptibility to hydrogen permeation of different microstructures of API X52 carbon steel, submitted to cathodic protection. The microstructures analyzed were obtained through heats treatments (water quenching and annealing). Therefore, the test was performed in base metal (BM), quenched base metal (QBM), annealed base metal (ABM) and weld metal (WM). The hydrogen permeation flow was evaluated using electrochemical tests in a Devanathan cell. The potentiodynamic polarization curves and electrochemical impedance were carried out to evaluate the corrosion resistance of each microstructure. All tests were carried out in synthetic soil solutions NS4 and NS4 + thiosulfate. The thiosulfate was used to simulate sulfate reduction bacteria (SRB). Through polarization and impedance, assays were established that the microstructure does not influence on the corrosion resistance. The permeation results showed that weld metal microstructure had lower hydrogen flow than the others microstructure permeated.

**Keywords:** Microstructure, Hydrogen Permeation tests, H<sub>2</sub>S, API 51 grade steel and cathodic protection.

### **Introdução**

The great challenges in increasing the oil and gas productions have been demanding more detailed studies related to the steels using for pipelines. Therefore, the knowledge about the mechanical behavior and microstructure of steels for manufacturing these pipelines is important to guarantee their integrity and safety conditions of operation [1, 2, 3, 4].

It requires a continual improvement of steels grade API 5L [5], for example, Han et al. [6] in their research proved that the welding procedure involved on the production of the pipes might modify the microstructure and properties of the base metal in the region of heat-affected zone (HAZ).

<sup>a</sup> Mestrando – UNIVERSIDADE FEDERAL DE SÃO JOÃO DEL REI

<sup>b</sup> Engenheiro Mecânico - UNIVERSIDADE FEDERAL DE SÃO JOÃO DEL REI

<sup>c</sup> Engenheiro Mecânico - UNIVERSIDADE FEDERAL DE SÃO JOÃO DEL REI

<sup>d</sup> PHD, Professor - UNIVERSIDADE FEDERAL DO RIO DE JANEIRO

<sup>e</sup> PHD, Professor - UNIVERSIDADE FEDERAL DE SÃO JOÃO DEL REI

The fractures related to "environmentally induced cracking," can be due the stress corrosion cracking (SCC) or hydrogen embrittlement (HE) mechanisms. In that case, some researchers believe that the process of external cracking of pipelines in contact with soil pH near neutral is associated to HE instead of SCC [1, 2, 3 and 4]. The hydrogen diffusion occurs differently in relation to the base metal and weld metal. Thus, it is important to study and compare this difference [1].

When the pipelines are exposed to aggressive environments with high cathodic protection, low pH and sulphate reduction bacteria, which are bacteria that use sulfate as an oxidizing agent, reducing it to sulfide ( $H_2S$ ), atomic hydrogen is produced on the metal surface. In presence of  $H_2S$ , the reaction of atomic hydrogen recombination to molecular hydrogen is retarded thereby permitting the diffusion through the metal [1]. It is well known that minimal amounts of  $H_2S$  are enough to result in materials which SCC and HE [7]. Another problem related to HE is because the steels, used in the manufacture of pipelines for transporting oil and their derivatives, are exposed to excessive cathodic protection. It puts the duct exposed to very low cathode potential where reduction of hydrogen on the metal surface becomes thermodynamically spontaneous [8, 9].

Therefore, any process which produces atomic hydrogen may cause absorption by the metal surface. A large amount of this hydrogen recombining results in the crystal lattice to form  $H_2$  bubbles under high pressure inside the metal. The initiation and propagation of cracks occur from these points of concentration of hydrogen [10].

The aim of this paper was to evaluate the influence of the microstructure on the susceptibility of hydrogen permeation of API X52 carbon steel submitted to the cathodic protection system. Different types of microstructures were obtained by quenching and annealing. The hydrogen permeation tests were evaluated in the presence of synthetic soil solution NS4 and modified solution NS4 + thiosulfate concentration of  $10^{-2}M$ .

## Metodologia

The pipeline material used was API X52 carbon steel, being welded joints and some base metal with different heat treatment. The evaluation of the chemical composition was carried out by Optical Emission Spectroscopy (OES).

The samples were heated at 900 °C for two hours. Quenching was performed in a solution of water, ice and salt. The annealed samples were left into the oven until it reaches room temperature. All the tests were performed in triplicate. The names and conditions adopted are listed on the table 1.

**Table 1 - Names and conditions of the samples.**

Sample name	Conditions
Base metal (BM)	As received
Annealed base metal (ABM)	Heated at 900 °C, cold in the oven
Quenching base metal (QBM)	Heated at 900 °C, cold in water, ice and salt

---

---

Weld metal (WM)

Removed from the welded joint of the pipeline as  
received

---

### **Metallographic analysis**

The metallographic analysis was performed according to Ballesteros [11]. The metallographic analyzes were carried out by Optical Microscopy (OM) and Scanning Electrochemical Microscopy (SEM) in order to evaluate the microstructures. The chemical attack was done using a solution of Nital 2% for 5 seconds. The samples designed for analysis of inclusions were evaluated without chemical attack.

The presence of the constituent Austenite-Martensite was determined by double electrolytic attack using the scanning electron microscopy (SEM). The following steps were adopted to the attack: 1) attack: 5 g EDTA, 0.5 g of NaF and 100 ml of distilled water at 5V for 15 seconds - 2) attack: 5 g of picric acid, 25 g NaOH and 100 ml of distilled water at 100 V for 5 sec.

### **Mechanical tests**

The hardness tests were conducted to supplement the materials characterization. These were performed on Rockwell B scale using sphere 1/16" with a load of 100 kg, and Rockwell C scale using diamond cone with a load of 150 kg.

### **Electrochemical tests**

The solutions used were a aerated naturally synthetic soil solution, called NS4 solution [12, 13], and used to simulate a synthetic soil, with pH around 8,4. The composition is (g/l): KCl: 0.122, NaHCO<sub>3</sub>: 0.483, CaCl<sub>2</sub>: 0.093 and MgSO<sub>4</sub>: 0.131

The other solution was the synthetic solution NS4 + thiosulfate, used to study the effect caused by sulfate-reducing bacteria [14]. It was prepared with a concentration of 10<sup>-2</sup>M of thiosulfate in the standard NS4 solution [12]. These solutions had initially a pH of 8.0 to 8.5.

The specimens for the electrochemical polarization and electrochemical impedance tests were cut, embedded in resin cold sandpaper and polished sequentially by 240, 400 and 600 grit sand paper. The cell used was a conventional three electrodes cell, being platinum as counter electrode, saturated calomel (SCE) as reference electrode and the working electrode (samples of API X52 carbon steel).

The scan rate adopted in the polarization curves was 1.0 mV.s<sup>-1</sup>, the applied potential range was -1.5 V to 0.5 V. The measurements were performed at room temperature (24 °C ± 3 °C) in naturally aerated solutions.

Electrochemical impedance measurements were performed in corrosion potential (E<sub>corr</sub>) in the frequency range of 10 mHz to 100 KHz, applying voltage with an amplitude of 10 mV and yielding 7 measures per decade of frequency.

The hydrogen permeation tests were carried out with the most aggressive solution, in that case the NS4 + thiosulfate. The hydrogen permeation was performed in a Devanathan cell [13, 15] using specimens with a thickness of 2 mm. Both sides of the steel specimen were in contact with different solutions controlled by independent potentiostats. The anodic side of the cell was filled with 1M NaOH solution and the cathodic side was filled with the NS4 + thiosulfate solution. The counter-electrode of the anodic side cell was attached to an amperimeter and a computer to measure the anodic current. Hydrogen permeation tests were carried out in the following steps:

1. Assemble the hydrogen permeation Devanathan cell containing the steel specimen.
2. 1M NaOH solution was introduced in the anodic side and the system was stabilized at the free corrosion potential.
3. Imposition of an anodic potential 100 mV above the free corrosion potential at the anodic side until the anodic passive current density became stable and below 1 A/cm<sup>2</sup>.
4. Introduction of NS4 solution in the cathodic side which remained at the free corrosion potential during 20 h.
5. Imposition of cathodic potential 300mV below the free corrosion potential during 24h. The test piece used was a flat plate of API X52 5L steel polished with diamond paste on both sides, with thickness and permeation section area constant.

The diffusion coefficient (D), in transient state, can be measured through Time Lag method, using the following equation:

$$D = \frac{L^2}{6t_l}$$

And it depends on the specimens thickness (L) and the time lag (t<sub>l</sub>), that is obtained from the time taken for permeation rate to reach 0.63 times the steady state value [16].

## Resultados e discussão

### Chemical analysis

The table 1 presents the results in percentage by weight of the chemical elements present in the base metal (BM) and the weld metal (WM).

**Table 1 - Chemical analysis of the base metal (BM) and the weld metal (WM).**

Material	Components (%)									
	C	Si	Mn	P	S	Cr	Ni	Mo	V	Cu
BM	0.28	0.33	1.11	0.03	0.02	0.05	0.02	0.01	ab 0.001	0.02
WM	0.16	0.20	0.47	0.03	0.03	0.03	0.02	0.15	0.002	0.02

The API 5L [5] classifies the carbon steel by the chemical composition and there are two types to specification based on the chemical elements present into the steel, named PSL1 and PSL2. The two PSL designations define different levels of standard technical requirements.

**Table 2 - Chemical composition according to specification in API 5L PSL2 standard.**

	<b>C</b>	<b>Mn</b>	<b>P</b>	<b>S</b>
<b>API 5L X52 PSL1</b>	0.260	1,400	0,030	0,030
<b>API 5L X52 PSL2</b>	0.220	1,400	0,025	0,015

Therefore, in relation to the 5L X52 PSL1 API specification (table 2), it concludes that the base metal does not reach the requirement of the standard API 5L PSL1 because of the deviations in relation to the minimum C and P contents (table 1). However, the weld metal is in accordance with this standard specification. Whereas if the classification is made by API 5L X52 PSL2 [5] (table 1), the nonconformity of the base metal is kept to the same elements, C and P, however with a larger deviation regarding to the minimum content and occurs also in relation to the S content. The weld metal is also in accordance with this standard specification.

### **Metallographic features**

The metallographic characterization was conducted in the API X52 carbon steel in the following conditions: Base metal (BM), weld metal (WM), annealed base metal (ABM) and quenched base metal (QBM).

The figure 1 is a scheme that indicates the positions where analyzes were performed with OM in the Base metal (BM), weld metal (WM). Base metal (Figure 2) has a heterogeneous distribution of ferrite and pearlite grains with grain boundaries well-defined. The same microstructure for the X52 steel was found in several other literatures [17, 18], possessing a ferritic-pearlitic combination.

The welded joint (weld metal, figure 3) presents a microstructure formed by low recrystallization, where it is possible to observe pearlitic microstructure and a decrease in the grain boundaries with degenerated pearlite regions. This fact was discussed by Park [2] and can be explained because the structure of degenerated pearlite phases, without the banding pattern, was different from pearlite evolved by normalizing and slow cooling treatment. The cooling rate in the weld metal was higher than necessary to form of typical pearlite, and thus the carbon diffusion during cooling was not sufficient to form the lamellar structure of cementite. This microstructural arrangement will be discussed later as one of the factors that influenced the results obtained for the permeation tests.

The figure 4 shows the Heat-Affected Zone (HAZ), where there is a great similarity with the microstructure of the BM; the little difference is due to the thermal effect caused by the deposition of the weld bead, which ultimately provides a grain growth microstructure of HAZ.



**Figure 1 - Photo of the weld zone of the API X52 carbon steel, with the positions that images were taken.**

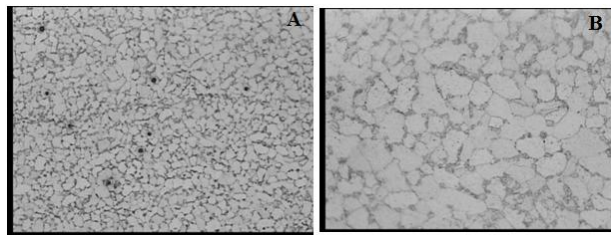


**Figure 2 - Position 3: Base Metal, image (A) zoom 200x and (B) 500x.**

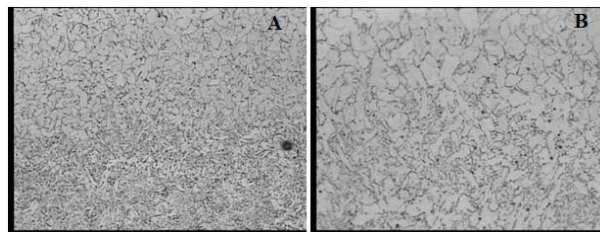


**Figure 3 - Position 4: Weld metal, image (A) zoom 200x (B) 500x.**

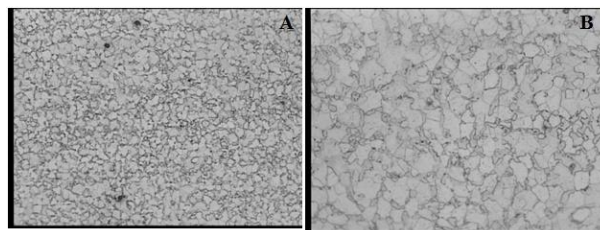


**Figure 4 - Position 5: Heat-Affected Zone, image (A) zoom 200x (B) 500x.**

The figure 5 presents the interface between WM and HAZ, presenting the difference between the microstructures. It is possible to observe that the HAZ presents major pearlite grains, showing the effect of heat treatment caused during the welding process. According to other authors [19], The HAZ generated by the welding thermal cycle showed a complex recrystallized microstructure located near the fusion line, formed by coarse-grained ferrite, acicular ferrite, small discontinuous pearlite colonies and some bainite grains.

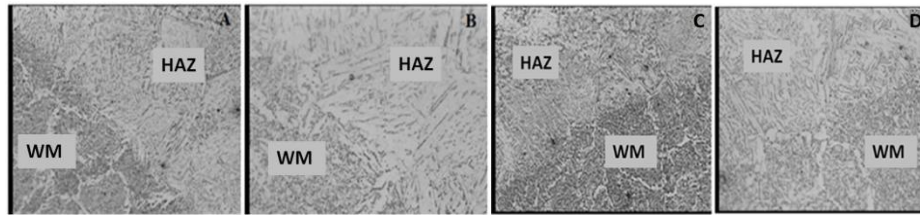


**Figure 5 - Positions 1 at the fig. 1: Interface weld metal and heat-affected zone, image (A) zoom 200x (B) 500x. Position 2 at the fig. 1: Interface weld metal and heat-affected zone, image (C) zoom 200x (D) 500x.**

The figures 6 and 7 show the microstructure after the heat treatment, being annealed base metal (ABM) and quenched base metal (QBM), respectively. It is possible to note the difference between the microstructure obtained. It is able to observe the presence of the pearlitic structure in the figure 6 (ABM); while the presence of martensite is noted in the quenched base metal - QBM (Figure 7).

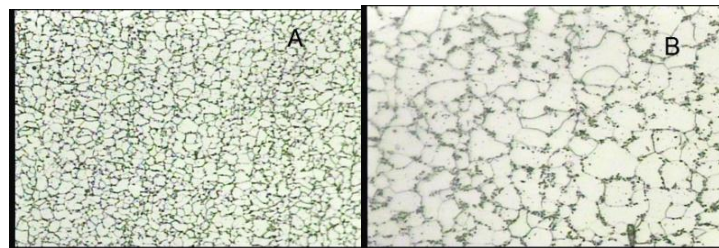


**Figure 6 - API X52, annealed base metal, zoom (A) 200x (B) 500x**

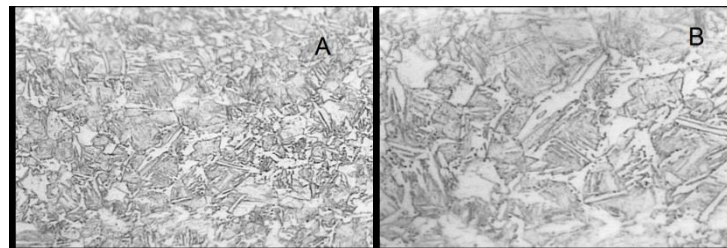


**Figure 7 - API X52, quenched base metal, zoom (A) 200x (B) 500x.**

Observations of the materials, without chemical attack, revealed the presence of a significant amount of inclusions, as shown on the figures 8 and 9.

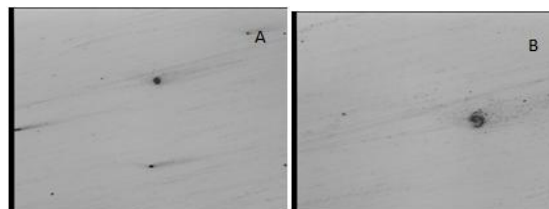


**Figure 8 – Base Metal without chemical attack, image (A) zoom 200x and (B) 500x.**

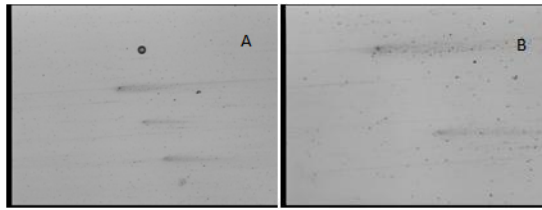


**Figure 9 – Weld Metal without chemical attack, image (A) and zoom 200x and (B) 500x.**

The EDS technique was used to evaluate the composition of these inclusions in order to verify the chemical elements present into the inclusions. The figures 10, 11 and 12 show these analyses. Therefore, the inclusions presented in API X52 carbon steel showed significant concentrations of S and Mn. Ayesha [16] has cited that MnS inclusions are considered strong irreversible trapping sites for hydrogen, working as follows: During the solidification of steel, Mn can combine with S giving rise MnS inclusions. The behavior of Inclusions/Matrix metal interface are reported in literature as strong trapping sites for hydrogen, consequently decreasing the hydrogen flux through the material.

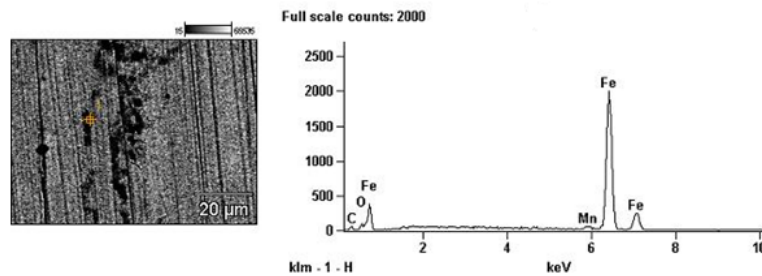


**Figure 10 - Analysis by EDS of inclusions present in the API X52 carbon steel.**

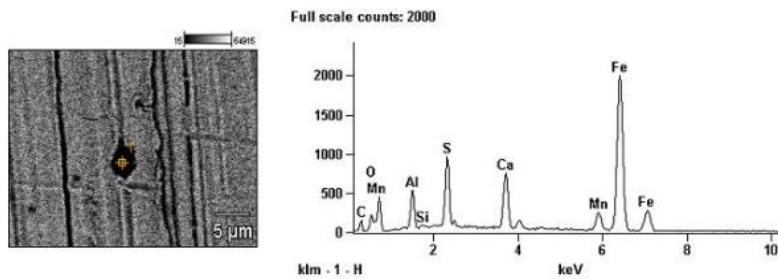


**Figure 11 - Analysis by EDS of inclusions present in the API X52 carbon steel.**

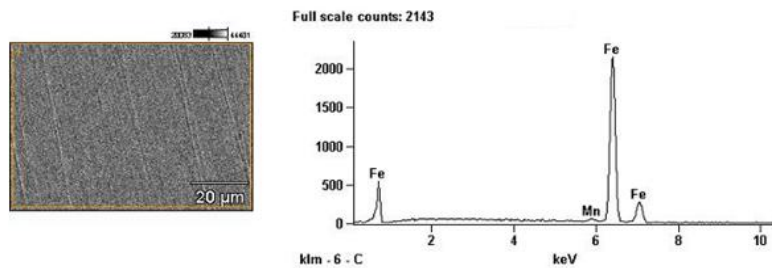


**Figure 12 - Analysis by EDS of area without inclusions in the API X52 carbon steel.**

The scanning electron microscopy (SEM) were performed at three different positions at the samples, as shown at the figure 13. The BM (Figure14-1) presents predominate phases of ferrite and pearlite. The HAZ and WM (Figure 14-2 and14-3) presents micro constituents of Austenite/Martensite. Called micro constituent A/M or micro phase A/M, they are regions of microscopic dimensions presented in C-Mn steels and low alloy that consist of cells stabilized austenite. The frequent presence, and high levels of martensite in these "islands" of austenite, derives its name Austenite-Martensite [20]. Chatzidouros [17] emphasizes that most pipeline steels are manufactured using thermo-mechanical processes that involve multiple heating and rolling stages which favors the formation of M/A constituents in low carbon steels. This micro constituent directly affects the tenacity of material due to your high hardness and fragility, the high density of discordances in the sub microstructure contributes to this formation [21].



**Figure 13 - Photo of the weld metal API X52 carbon steel, with the positions of the captured images.**

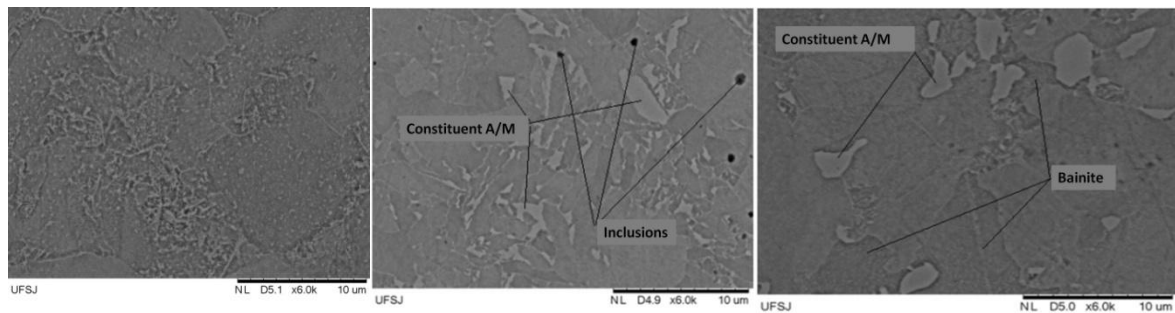


**Figure 14 - Position 1: Image of Base Metal zoom 5000x.. Position 2: Image of Weld Metal zoom 5000x, showing the constituent A / M and the inclusions. Position 3: Image of the heat-affected zone zoom 5000x, showing the constituent A / M and regions formed by bainite.**

After heat treatments, the SEM analyzes show that the grains of pearlite were more defined and have a little increase in the samples of annealed base metal, as showed in the figure 15 (A). The quenched base metal specimens had presented martensitic structure, but due to the low carbon have noted some grain of ferrite, as proved in the figure 15 (B).

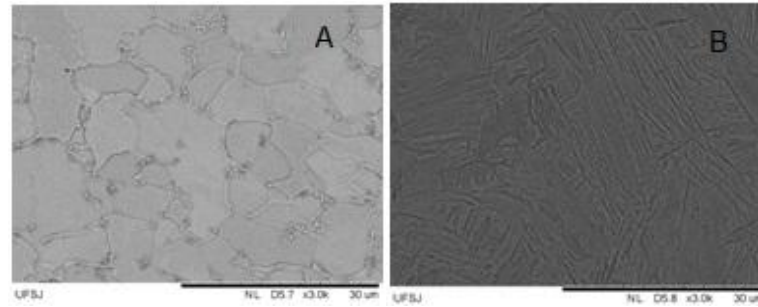


**Figure 15 - Image of Base Metal after two different heat treatments. Annealed (A), and quenched (B), zoom 3000x.**

The hardness tests were performed to complement the materials characterization, as shown in Table 6.

**Table 6 - Measures hardness of the samples studied.**

API X52 – BM	84 HRB
API X52 – WM	80 HRB
API X52 – ABM	67 HRB
API X52 – QBM	24 HRC

## Polarization

The cathodic and anodic polarization curves obtained in solutions NS4 and NS4 + thiosulfate with a concentration of 10-2M are shown in the figures 16 and 17. The anodic current density was highest for NS4 + thiosulfate solution, it may be attributed to reduction reaction of thiosulfate that converted into H<sub>2</sub>S [22]. Thus, the electrochemical tests for the specimens ABM and QBM were performed only in this solution, that was more aggressive (figure 17 and table 8).

The tests were performed in naturally aerated condition. The table 7 shows the corrosion potentials ( $E_{corr}$ ) in each test condition as well as the values of current density at 50mV and 100mV (SCE) above Corrosion potential ( $E_{corr}$ ).

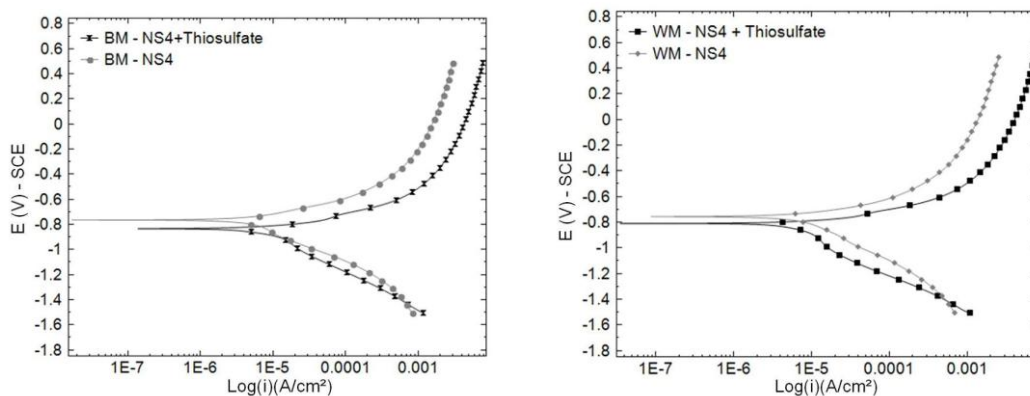


**Figure 16 - Anodic and cathodic polarization curves of the base metal (BM) and weld metal (WM) of the API X52 carbon steel immersed in the NS4 synthetic soil solution and NS4 + thiosulfate modified  $10^{-2}M$ .**

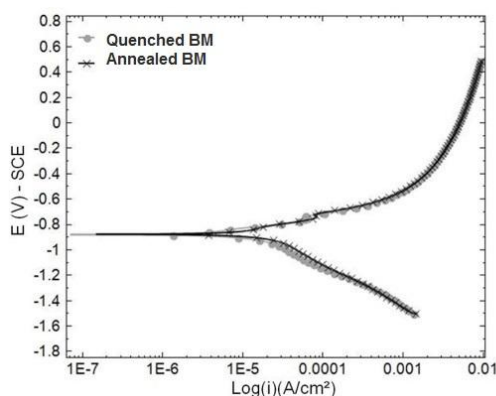


**Figure 17 - Anodic and cathodic polarization curves of the annealed base metal (ABM) and quenched base metal (QBM) of the API X52 carbon steel immersed in the NS4 + thiosulfate modified 10-2M solution.**

All the samples showed active dissolution in all tested conditions. Therefore, it was not observed any domain of passivation in a range of 700 mV of anodic polarization, similar results were obtained for Bueno in previous works, [3, 4, 14 and 23]. It is also observed that the corrosion potential do not vary between the specimens BM, WM, ABM and QBM.

The cathodic currents density observed, in all tests, can be attributed to the reduction reactions of hydrogen and oxygen. Based on the Pourbaix electrochemical equilibrium diagram for the system Fe/H<sub>2</sub>O, at 25°C [9], all the specimens, in both solutions, presented corrosion potentials under naturally aerated conditions, which were within the domain of corrosion and below the equilibrium line H/H<sup>+</sup>. In this case, the reactions of Fe/Fe<sup>2+</sup> anodic dissolution and reduction of hydrogen are thermodynamically spontaneous. Thus, all of samples showed effect of active dissolution, being within the domain of corrosion with solubility of Fe<sup>2+</sup> ion, as well as the reaction of hydrogen reduction on the metal surface.

Analyzing the Figures 16 and 17 can be seen that the corrosion potential ( $E_{corr}$ ) to NS4 + thiosulfate solution for all samples ranged around an average value of -0.758 mV. The current density in anodic polarization curves presented similar behavior. It is the conclusive proof that different microstructures have no significant effects about corrosion resistance, but the thiosulfate addition initially generates the reduction of corrosion potential in relation to the NS4 standard solution. It is possible to note that a significant variation of the current occurred when the thiosulfate was added, showed on table 7. It can be stated that the addition of thiosulfate accentuated the corrosion process, anodic current increase with respect to the solution without thiosulfate. It proves that the solutions with thiosulfate presented a corrosion potential more anodic, becoming more aggressive, which evidence the results obtained in the polarization curves.

Using the data in Table 7 and Figures 16 and 17, it is possible to note that the anodic current densities increase in relation to the applied potential above 50 mV and 100 mV of the  $E_{corr}$ ,

proving that all samples presented active dissolution. According Pourbaix [9], the region between  $E_{corr}$  to pH 8.5, the specimens take place in the domain of stability of the  $Fe^{2+}$  ion, occurring active dissolution of the metal.

**Table 7 – Corrosion potential ( $E_{corr}$ ), current density at 50mV and 100mV above the corrosion potential.**

		pH	$E_{corr}$ (ECS)	E 50mV above $E_{corr}$	i 50mV above $E_{corr}$ ( $\mu A/cm^2$ )	E 100mV above $E_{corr}$	i 100mV above $E_{corr}$ ( $\mu A/cm^2$ )
<b>BM</b>	<b>NS4</b>	8.4	-0.716	-0.666	2.597E-5	-0.616	6.796E-5
	<b>NS4+thiosulfate</b>	8.6	-0.766	-0.716	8.847E-5	-0.667	2.175E-4
<b>WM</b>	<b>NS4</b>	8.1	-0.695	-0.645	6.247E-5	-0.595	1.185E-4
	<b>NS4+thiosulfate</b>	8.8	-0.758	-0.708	7.617E-5	-0.658	2.105E-4
<b>QBM</b>	<b>NS4+thiosulfate</b>	7.9	-0.743	-0.692	1.125E-4	-0.642	3.231E-4
<b>ABM</b>	<b>NS4+thiosulfate</b>	8.3	-0.766	-0.717	8.401E-5	-0.667	2.568E-4

### Electrochemical impedance

The results of EIA for base metal (BM) and weld metal (WM) in the NS4 synthetic soil solution and NS4 + thiosulfate with concentration of 10-2M are shown in the figures 18,19. The figure 20 presents the EIS for the annealed base metal (ABM) and quenched base metal (QBM) in NS4 + thiosulfate with concentration of 10-2M.

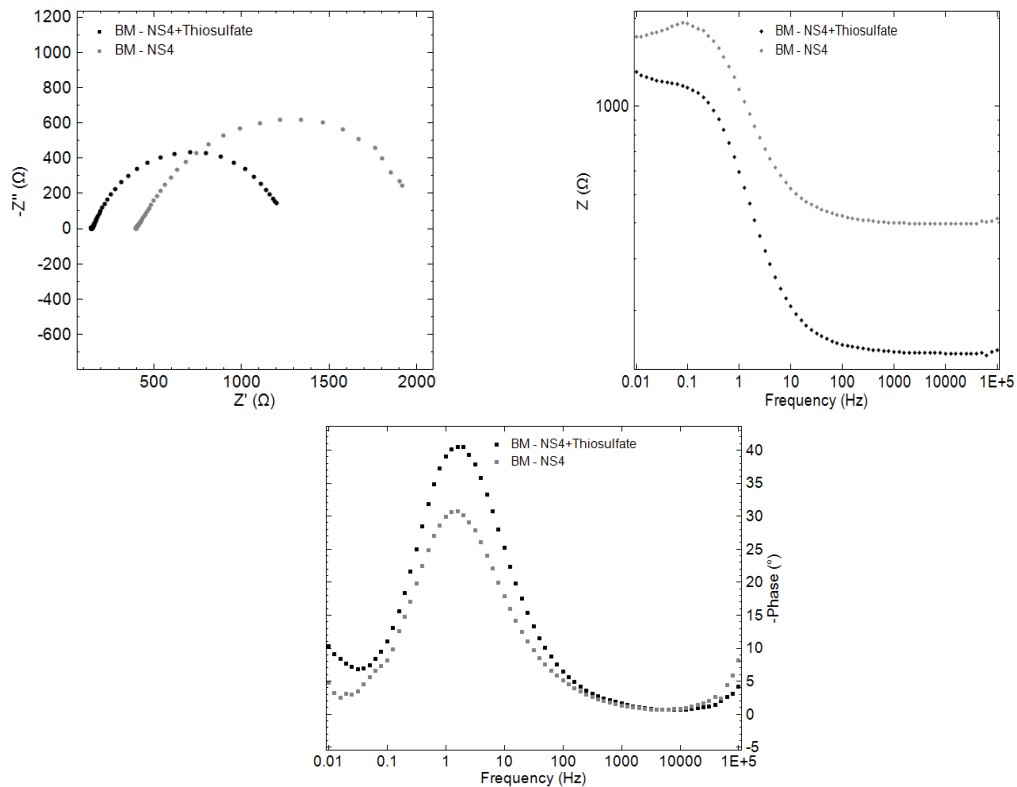


**Figure 18 - Nyquist diagrams (upper left), Bode module (upper right) and Bode phase angle (bottom) for the base metal of the API X52 carbon steel immersed in NS4 synthetic soil solution and modified solution of NS4 + thiosulfate 10-2M.**

The Nyquist diagram shows an increased capacitive arc when using the less aggressive solution (NS4) and Bode shows a large decreasing in impedance when using the solution NS4 + thiosulfate. On the diagram module Bode notes a significant decreasing in impedance at low frequencies when using the solution NS4 + thiosulfate. This might suggest a decreasing in corrosion resistance of steel in the presence of thiosulfate.

These results are in agreement with those obtained in polarization curves where higher anodic current density was obtained in assays performed with the solution of NS4 + thiosulfate, both as to BM, WM. The diagram Bode phase angle indicates no major changes according to immersion time.

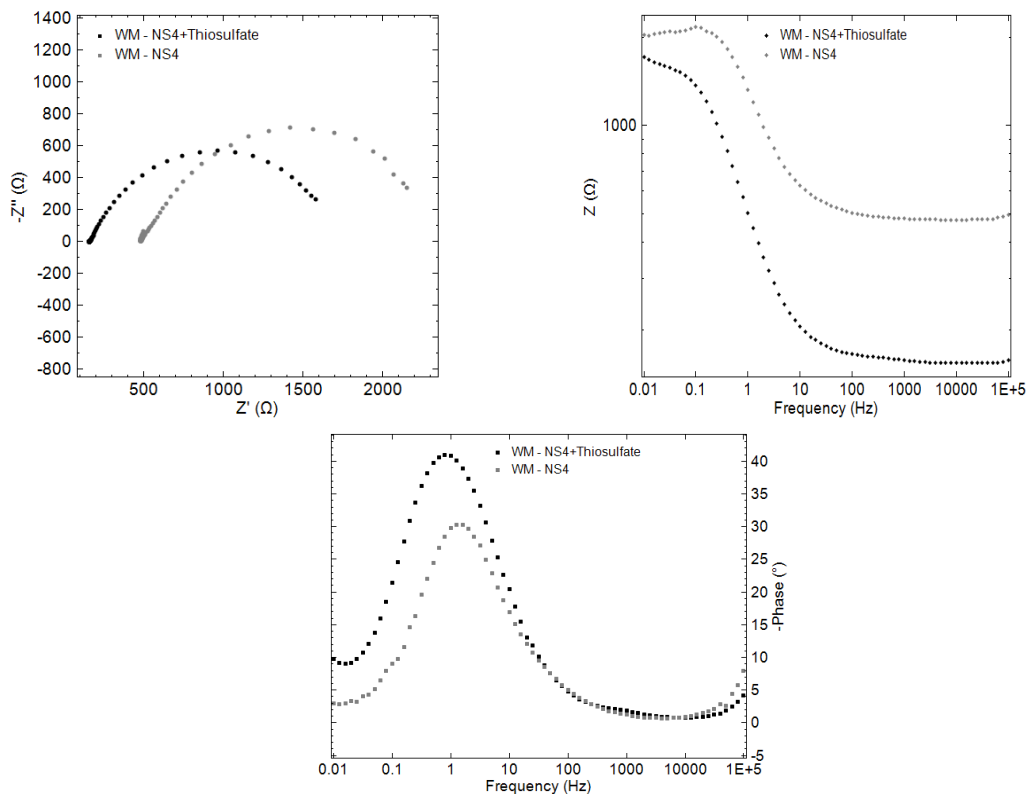


**Figure 19 - Nyquist diagrams (top left), Bode Module (top right) and Bode phase angle (bottom) to the weld metal of the API X52 carbon steel immersed in NS4 synthetic soil solution and modified solution of NS4 + thiosulfate 10-2M.**

The figure 19 shows the Nyquist diagrams indicates an increasing in capacitive arc, and Bode already indicates increasing impedance at low frequencies to NS4 solution, which would suggest an increase in corrosion resistance of steel in this solution. The Bode diagram phase angle reveals that the mechanisms for the steel in both solutions are similar. These results confirm those obtained in polarization curves and are similar to those for the BM. As previously evidenced the higher aggressivity of solution NS4+thiosulfate, samples heat treated were tested only in this solution and the figure 20 shows the results.

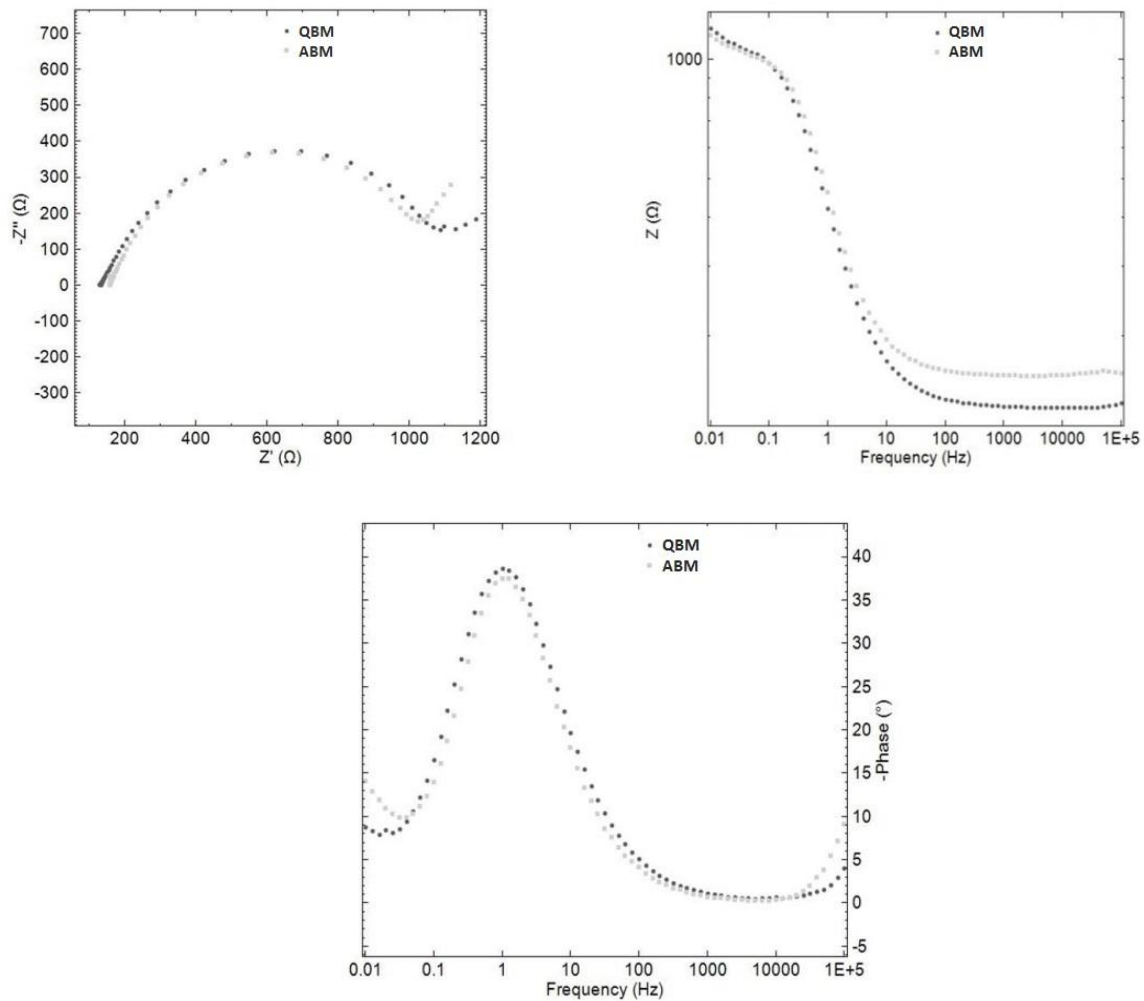


**Figure 20 - Nyquist diagrams (top left), Bode Module (top right) and Bode phase angle (bottom) to the annealed base metal (ABM) and quenched base metal (QBM) of the API X52 carbon steel immersed in modified solution of NS4 + thiosulfate 10-2M.**

Nyquist diagrams show that both samples, ABM and QBM, had the same behavior. The capacitive arcs are very similar showing the same impedance module from the lower frequencies up the highest. With the Bode module diagram can be observed practically the same impedance value at low frequencies, but in higher frequencies occurs a decrease in ABM impedance. The mechanism in Bode phase diagram is equal for both, showing the highest phase angles in the medium frequencies region. Through these data and observations it is clear that the heat treatments performed did not affect the corrosion resistance of the material.

All of impedance values were measured in the frequency of 0,12589 Hz, as shown on table 8. In that case, it is possible to note that the microstructure did not affect the corrosion resistance of the API X52.

**Table 8 - Values of impedance obtained for all conditions, frequency of 0.12589 Hz.**

Frequency (Hz)	Impedance (ohm)
----------------	-----------------

BM	NS4	0,12589	1879,3
	NS4+thiosulfate	0,12589	1137,7
WM	NS4	0,12589	2161,9
	NS4+thiosulfate	0,12589	1297,9
ABM	NS4+thiosulfate	0,12589	1198,72
QBM	NS4+thiosulfate	0,12589	1202,92

## Hydrogen permeation

The figure 21 presents the test permeation of all specimens. Tests were performed by hydrogen permeation using the more aggressive solution, namely NS4 + thiosulfate, already evidenced in polarization and electrochemical impedance tests. The permeation tests with cathodic potential applied of -1.5 V below  $E_{corr}$  were carried out in order to simulate cathodic protection system, once ISO 15589-1 [13] describes that from values lower than -1.2V the steel already suffering effects of hydrogen embrittlement.

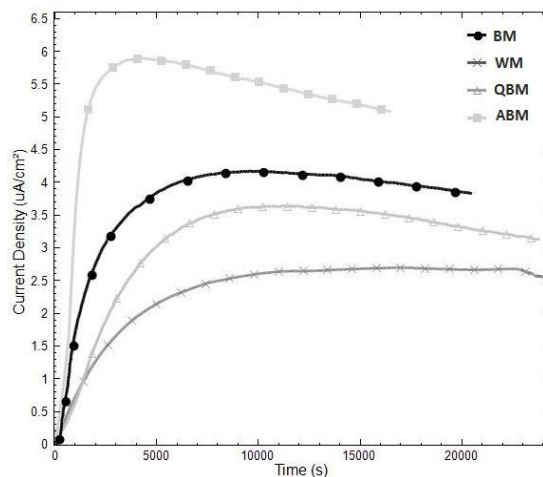


**Figure 21- Hydrogen Permeation, base metal (BM), weld metal (WM), annealed base metal (ABM) and quenched base metal (QBM) of API X52 carbon steel in the modified solution NS4 + thiosulfate 10-2 M.**

The solution NS4 + thiosulfate was able to induce absorption and permeation of hydrogen in all materials tested. The reduction process converts thiosulfate to H<sub>2</sub>S [14]. In that case, the effect of H<sub>2</sub>S does not allow H<sub>0</sub> turns into H<sub>2</sub>. Due to the addition of thiosulfate, the potential of the cathode side in contact with the steel were located within the domain of stability of H<sub>2</sub>S (Figure 22). Therefore, there is an increase in the activity of ions and reduction hydrogen on the steel surface [15]. As found in the literature, there are different factors that involve the flow of hydrogen through the material as well as cited below.

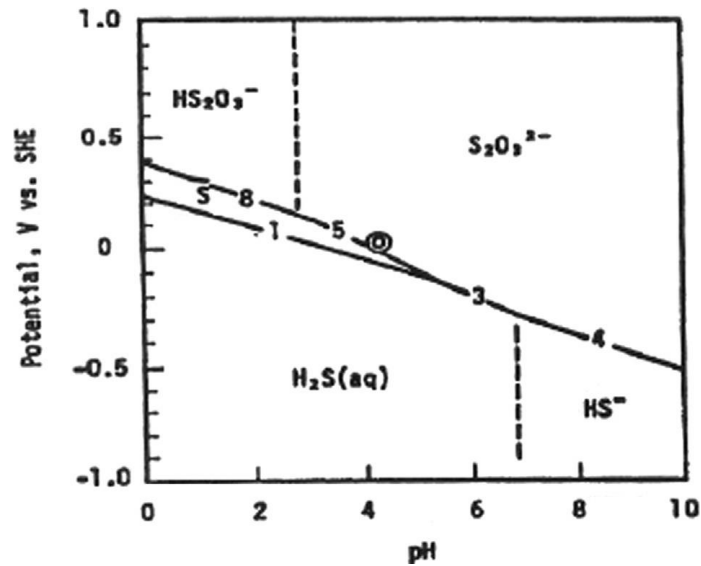


Figure 22 - E vs. pH for thiosulfate and H<sub>2</sub>S thermodynamic equilibrium in aqueous solutions [11].

During initial stage, the permeation process resembles a stationary permeation behavior, but in a second stage occurs a progressive increase of current with as time goes by. This difference in the current flow is probably due to the microstructural characteristics, like the carbide form and size of grains differentiated between the different studied conditions [1, 2 and 24]. It is shown more detailed below.

The goal of the heat treatment is to modify the structural arrangement of the carbides (Fe<sub>3</sub>C) which assume different forms for each one. As shown by Nagu and Ramunni [25, 26] changes in the carbide morphology of low carbon steels do significantly alter the permeability, the diffusion constant, and the apparent solubility of hydrogen. The hydrogen diffusion coefficient in steel matrix generally is very low at low temperatures. In that case, most of hydrogen is retained not in the unit cells interstices but in different sites commonly called traps. These traps have been related to microstructural features such as dislocations, interfaces, vacancies, impurity atoms, micro voids or any other lattice defect [3, 4, 5 and 8]. The trap densities are inversely proportional to the diffusion coefficients. [16]

There are reports in the literature that affirm that Mn, S and other inclusions, as showed in figure 10 and 11, are some of the reasons that contribute to variance the ease with which the hydrogen is solubilized or diffused metallic materials solid at room temperature, [8, 27] and other reasonable possibility is that carbides act as obstacles to diffusion of hydrogen [1].

The data of the permeation tests are listed in table 9 that brings the highest density current, the time necessary to reach it and the diffusion coefficient.

Table 9 - Values of permeation in different microstructures of API X52 carbon steel.

Microstructure/sample	Highest density current (uA/cm <sup>2</sup> )	Time (s)	Diffusion coefficient (D) (mm <sup>2</sup> /s)
ABM	5,9101	4320	2,45x10 <sup>-4</sup>
BM	4,1086	10320	1,02x10 <sup>-4</sup>
QBM	3,6555	11220	0,94x10 <sup>-4</sup>

<b>WM</b>	2,7130	16950	0,24x10 <sup>-4</sup>
-----------	--------	-------	-----------------------

These data shows the difference between the permeation in the different microstructures. ABM has the highest current density in a lowest time, the QBM and WM even with biggest times showed smallest permeation values, all permeation results will be discussed below.

### **ANNEALED BASE METAL**

The highest hydrogen flux occurred in the ABM samples as proved in figure 21 and table 8. Annealed samples showed the micrographs (Figure 6 and 15) considerable grain growth of ferrite and pearlite formation at the edges. Consequently, this microstructure with large difference atomic arrangement of its unit cells was the condition that caused the increase of the hydrogen flow through the material. The annealed microstructure presented on figures 6 and 15, had lower discordances density than others samples. Therefore, according to Ayesha [16] ferrite grains exhibited the highest diffusivity in samples. In addition, Svoboda [28] confirmed that the annealing thermal treatment was probably sufficient to recover the majority of defects, decreasing the discordance density and only a small amount of them survived. Therefore, the hydrogen atom found less difficulty to pass through the metal. This fact was also confirmed by other authors [6].

### **BASE METAL**

Base metal was essayed as received, their micrographs showed similar microstructure in relation to ABM, ferrite grains with pearlite formation in the edges. However, it can be seen the difference between the grains size. In that case, it is not possible to affirm what heat treatment the BM was submitted during its production, but it can be noted the smaller grain size compared to ABM, which was submitted to a heat treatment at the laboratory.

For this reason, because of the small size grain in relation to ABM, it causes an increase of discordances and defects, increasing the hydrogen trap density inside the metal and decreasing the hydrogen diffusion coefficient (table 9). In that case, BM had the second highest rate of hydrogen permeation. Han [6] found similar results and concluded that equiaxed ferrite grains and pearlite, as presented in BM, favors the diffusivity of hydrogen due the low trap density.

### **QUENCHED BASE METAL**

The tests conducted on the QBM that are possible to see in the figure 21 and in the table 9, had lower current flow and enhance the time to reach a stationary value to permeation than the ABM and BM. Similar results were obtained for Nagu [25], the quenched material had martensitic inter-lath interfaces, high density of dislocations and carbide–matrix interfaces all of which act as hydrogen traps. These traps were apparently effective in delaying hydrogen transport as those in the as-received steel. This behavior is probably due to the difference in grain size caused by thermal treatments performed and generated several changes in the structure of the material. The fastest cooling rate during heat treatment process promotes the transformation to martensite at lower temperature with an increase in dislocation density, arising from the transformation volume change.

Considering that the dislocations act as traps for hydrogen, the combined effect of a lower grain size and higher dislocation density could result in the lower diffusivity of hydrogen. It is known that the samples quenched have martensitic microstructure which has its atomic arrangement in TCB form (tetragonal centered body). Therefore, stable phases at room temperature (ferrite and cementite) cannot be formed due to the rapid cooling, differently from the annealed samples and the base metal that present a mixture of ferrite/cementite (pearlite), and grains of ferrite CCB (body centered cubic) [29].

The found results are according to the literature, where Luu [30] also proves that lower permeation and diffusivity of hydrogen occurs in martensitic microstructure due to high density of defects and discontinuities imposed by rapid cooling. In addition, also to the fact that the matrix is saturated with carbon that does not completely diffuse. For this reason, these combinations of factors act as traps and significantly decrease the hydrogen flow. Lippo [31] also reported similar results, affirming that the hydrogen diffusivity attains a minimum value in a fresh martensite because of the high density of lattice imperfections introduced by martensitic structure. Therefore, it is confirmed that the martensitic transformation acts as traps for diffusing hydrogen atoms and consequently a decrease in diffusivity and hydrogen permeation flux.

## **WELD METAL**

The WM samples showed the lowest permeation rate of all analyzed samples, as can be seen on the table 9 and the figure 21.

Due to melting and solidification process during the weld, the weld metal microstructure is changed. In that case, the recrystallization and uncontrolled grain growth in the heat affected zone (HAZ), caused by thermal cycles, increase the density of discordance. Furthermore, these processes contribute to many factors such as: large changes in the microstructure due to the spot heat incidence, phase additions, phases changes, precipitation, residual stresses, discontinuities in the matrix and many others according to Han [6].

It is believed that these are the reason for the lowest diffusion coefficient (table 9) due a huge number of discordances that works to retard the hydrogen diffusion [2, 16, 32, 33, 34]. Moreover, the presence of inclusions has an important role to hold the hydrogen [16]. Variations of microstructure and a significant presence of inclusions are showed in the metallographic analysis of WM in HAZ, figure 14. In that case, the WM region is an area with high number of traps of various types that retains the hydrogen during the permeation process. Han [6] concluded that the microstructure of different zones in the welded joints can be affected by different welding heat input, consequently it can shows very different hydrogen permeation behavior. It was also observed to Han that the base metal had the highest hydrogen permeation rate. The WM showed the lowest values.

## **Conclusões**

---

1- The solution NS4 + thiosulfate showed more aggressiveness than standard NS4 solution. This behavior was probably caused by the effect of sodium thiosulfate. In that case, it was observed a higher current density in the anodic polarization curves with thiosulfate and lower polarization resistance test results in impedance.

2- The biggest change in the microstructure was observed in the weld joint. The metallographic characterization showed that the API X52 steel - BM has a heterogeneous distribution of ferrite and pearlite grains with grain boundaries well-defined. The API X52 steel - welded joint microstructure showed a structure formed by a low recrystallization where can be realize an increase in pearlite microstructure and a decrease in the grain boundaries. The QBM presents a well-defined martensite in microstructure while the ABM samples demonstrated a significant increase in grain size of ferrite.

3- As reported in the literature, the samples did not show different resistances to corrosion even with the changes of the microstructure, proving that thermal treatments did not influence on the corrosion resistance.

4- According to the analysis by SEM was found some inclusions present in API X52 steel, showing significant concentrations of S and Mn. Consequently, these can be a significant factor influencing the values of hydrogen permeation.

5- The low permeation and diffusivity of hydrogen occurred in martensitic microstructure is due to high density of defects and discontinuities imposed by rapid cooling. In addition, also to the fact that the matrix is saturated with carbon that does not completely diffuse. For this reason, these combinations of factors act as traps and significantly decrease the hydrogen flow. In that case, the quenched material had martensitic inter-lath interfaces, high density of dislocations and carbide–matrix interfaces all of which act as hydrogen traps.

6- The WM samples showed the lowest permeation rate of all analyzed samples as can be seen on de diffusion coefficient calculation. It probably occurred because of melting and solidification process during welding; the weld metal microstructure was changed. In that case, the recrystallization and uncontrolled grain growth in weld metal and in the heat affected zone (HAZ), caused by thermal cycles, increase the density of discordance. It is believed that the lowest rate permeation occurred because of a huge number of discordances and inclusions that works to retard the hydrogen diffusion.

### **Referências bibliográficas**

---

[1] BUENO, A. H. S.; PONCIANO, J.A.C. “Plano de gerenciamento de integridade de dutos contra corrosão. CORROÇÃO E PROTEÇÃO”. V. 5, N. 22-3, P. 23-8, JUL/AGO. 2008.

[2] GYU TAE PARK, SUNG UNG KOH, HWAN GYO JUNG, KYOO YOUNG KIM. “Effect of microstructure on the hydrogen trapping efficiency and hydrogen induced cracking of pipeline steel”. Corrosion Science, Volume 50, July 2008, Pages 1865-1871.

[3] BUENO, A. H. S., MOREIRA, E. D., GOMES, J. A. C. P., “Evaluation of stress corrosion cracking and hydrogen embrittlement in an API grade steel”. Engineering Failure Analysis (2013). v. 1, p. 1, 2013.

[4] BUENO, A. H. S., CASTRO, B. B., PONCIANO, J. A. C., “Assessment of stress corrosion cracking and hydrogen embrittlement susceptibility of buried pipeline steels”. Environment-Induced Cracking of Materials, Volume 2, 2008, Pages 313-322.

[5] API 5L, API Specification for Line Pipe, American Petroleum Institute, Washington, DC, July 2000.

- 
- [6] HAN, Y. D., JING, H.Y., XU, L.Y., “Welding heat input effect on the hydrogen permeation in the X80 steel welded joints”. *Materials Chemistry and Physics*, Volume 132, 16 January 2012, Pages 216-222.
- [7] A. CONTRERAS, A. ALBITER, M. SALAZAR, R. PÉREZ, “Slow strain rate corrosion and fracture characteristics of X-52 and X-70 pipeline steels”. *Materials Science and Engineering: A*, Volume 407, 25 October 2005, Pages 45-52.
- [8] D. HARDIE, E. A. CHARLES, A. H. LOPEZ, “Hydrogen embrittlement of high strength pipeline steels”. *Corrosion science*, p. 4378-4385, 2006.
- [9] POURBAIX, M., *Atlas of electrochemical equilibrium in aqueous solutions*, Nace International, 2<sup>a</sup> ed., Cebelcor, Bélgica, 1974.
- [10] GENTIL, V., *Corrosão*. 6<sup>a</sup> Ed., p. 154-165, 2011.
- [11] BALLESTEROS, A. F., PONCIANO, J. A. C., SOBOOT, I. “Susceptibilidade de juntas soldadas circunferenciais de aço API 5L X80 à corrosão sob tensão e à fragilização por hidrogênio”. *Tecnol. Metal. Mater. Miner.*, vol.6, n<sup>o</sup>.3, p. 147-152, 2010.
- [12] PARKINS, R. N., BLANCHARD, W. K. AND DELANTY, B. S., “Transgranular Stress Corrosion Cracking of High-Pressure Pipelines in Contact With Solutions of Near Neutral pH”. *Corrosion*, V. 50, N. 5, PP. 394 – 408, 1994.
- [13] ISO 15589-1, *Petroleum and natural gas industries - Cathodic protection of pipeline transportation systems - Part 1: On-land pipelines*, 2003.
- [14] SIQUEIRA, P. T., BUENO, A. H. S, PONCIANO, J. A C. G, “Effect of cathodic potential on hydrogen permeation of API grade steels in modified NS4 solution”, in: ICC – International corrosion congress, China, 2005.
- [15] DEVANATHAN, M. A. V. and STACHURSKI, Z. *Proc. Roy. Soc.*, A270, 90 1962.
- [16] AYESHA J. HAQ\*, MUZAKA, K., DUNNE, D.P., CALKA, A., PERELOMA, E.V., “Effect of microstructure and composition on hydrogen permeation in X70 pipeline steels”. *International Journal of Hydrogen Energy*, Volume 38, 19 February 2013, Pages 2544-2556.
- [17] CHATZIDOUROS, E.V., PAPAZOGLU, V.J., PANTELIS, D.I., “Hydrogen effect on a low carbon ferritic-bainitic pipeline steel”. *International Journal of Hydrogen Energy*, Volume 39, 31 October 2014, Pages 18498-18505.
- [18] NANNINGA, N.E., LEVY, Y.S., DREXLER, E.S., CONDON, R.T., STEVENSON, A.E., SLIFKA, A.J., “Comparison of hydrogen embrittlement in three pipeline steels in high pressure gaseous hydrogen environments”. *Corrosion Science*, Volume 59, June 2012, Pages 1-9.

- [19] VARGAS-ARISTA, B., HALLEN, J. M., ALBITER, A., “Effect of artificial aging on the microstructure of weldment on API 5L X-52 steel pipe”. *Materials Characterization*, Volume 58, August–September 2007, Pages 721-729.
- [20] REBELLO, J. M. A., SOUR, A., “O constituinte austenita-martensita (AM)”. *Resumo – Universidade Federal do Rio de Janeiro*, Rio de Janeiro. p. 19, 1996.
- [21] ROBERTO, S. B., “Análise microestrutural de junta soldada de aço baixa liga”. *Resumo COPPE – Universidade Federal do Rio de Janeiro*, Rio de Janeiro, 2010.
- [22] BUENO, A. H. S., 2007, “Avaliação integrada de mecanismos de falha por corrosão em dutos”, tese de D. Sc., COPPE/UFRJ, Brasil.
- [23] BUENO, A. H. S., GOMES, J. A. C. P., “Environmentally induced cracking of API grade steel in near-neutral pH soil”. *Journal of the Brazilian Society of Mechanical Sciences and Engineering*, v. 31, p. Apr.\June 2009, 2009.
- [24] HUANG, F., LIU, J., DENG, Z. J., CHENG, J. H., LU, Z. H., LI, X. G., “Effect of microstructure and inclusions on hydrogen induced cracking susceptibility and hydrogen trapping efficiency of X120 pipeline steel”. *Materials Science and Engineering: A*, Volume 527, 15 October 2010, Pages 6997-7001.
- [25] NAGU, G. A., AMARNATH, NAMBOODHIRI, T. K. G., “Effect of heat treatments on the hydrogen embrittlement susceptibility of API X65 grade line-pipe steel”. *Indian Academy of Sciences*, nº.4, vol. 26, p. 435-439, 2003.
- [26] RAMUNNI, V. P., COELHO, T. P., MIRANDA, P. E. V., “Interaction of hydrogen with the microstructure of low-carbon steel”. *Materials Science and Engineering: A*, Volumes 435–436, 5 November 2006, Pages 504-514.
- [27] OLIVEIRA, J. R, 2007, “Aplicação de métodos eletroquímicos para determinação da corrosividade do solo”, tese de Msc, COPPE/UFRJ, Brasil.
- [28] SVOBODA, J., MORI, G., PRETHALER, A., FISCHER, F.D., “Determination of trapping parameters and the chemical diffusion coefficient from hydrogen permeation experiments”. *Corrosion Science*, Volume 82, May 2014, Pages 93-100.
- [29] CALLISTER, W. D., *Ciência e engenharia de materiais, uma introdução*. 7ª ed., p. 456-477, 2008.
- [30] LUU, W.C., WU, J.K. “The influence of microstructure on hydrogen transport in carbon steels”. *Corrosion Science*, Volume 38, Issue 2, February 1996, Pages 239-245.
- [31] LUPPO, M. I., OVEJERO-GARCIA, J. “The influence of microstructure on the trapping and diffusion of hydrogen in a low carbon steel.”. *Corrosion Science*, Volume 32, 1991, Pages 1125-1136.

[32] ALVARO, A., OLDEN, V., MACADRE, A., ODD MAGNE AKSELTEN, “Hydrogen embrittlement susceptibility of a weld simulated X70 heat affected zone under H<sub>2</sub> pressure”. *Materials Science & Engineering A* 597 (2014) 29–36

[33] BUENO, A. H. S. ; GOMES, J. A. C. P. “Environmentally induced cracking of API grade steel in near-neutral pH soil”. *Journal of the Brazilian Society of Mechanical Sciences and Engineering (Impresso)*, v. 31, p. Apr.\June 2009, 2009.

[34] BUENO, A. H. S. ; GOMES, J. A. C. P. “Assessment of Stress Corrosion Cracking and Hydrogen Embrittlement Susceptibility of Buried Pipeline Steels”. In: Sergei Shipilov, Russell Jones, Jean-Marc Olive e Raúl Rebak. (Org.). *ENVIRONMENT-INDUCED CRACKING OF MATERIALS*. 1ed.: Elsevier, 2007, v. 2, p. 313-322.

\* \* \*